Metrol. Meas. Syst., Vol. 26 (2019) No. 3, pp. 449–461
DOI: 10.24425/mms.2019.129581

METROLOGY AND MEASUREMENT SYSTEMS
Index 330930, ISSN 0860-8229
www.metrology.pg.gda.pl

MEASUREMENT OF RETINA VESSELS BY SEGMENTATION OF IMAGES RECONSTRUCTED FROM OPTICAL COHERENCE TOMOGRAPHY DATA

Tomasz Marciniak[1)], Agnieszka Stankiewicz[1)], Adam Dąbrowski[1)], Marcin Stopa[2, 3)], Piotr Rakowicz[2, 3)], Elżbieta Marciniak[2, 3)]

1) *Poznań University of Technology, Institute of Automation and Robotics, Piotrowo 3a, 60-965 Poznań, Poland* (*tomasz.marciniak@put.poznan.pl*, ✉ *agnieszka.stankiewicz@put.poznan.pl*, +48 61 647 5945, *adam.dabrowski@put.poznan.pl*)
2) *Poznań University of Medical Sciences, Chair of Ophthalmology and Optometry, Rokietnicka 5D, 60-806 Poznań, Poland* (*stopa@ump.edu.pl, rakowicz@ump.edu.pl, marciniak@ump.edu.pl*)
3) *Poznań University of Medical Sciences, Clinical Eye Unit and Pediatric Ophthalmology Service, Heliodor Święcicki Medical Hospital, Grunwaldzka 16/18, 60-780 Poznań, Poland*

Abstract

In this paper methods and their examination results for automatic segmentation and parameterization of vessels based on spectral domain optical coherence tomography (SD-OCT) of the retina are presented. We present three strategies for morphologic image processing of a fundus image reconstructed from OCT scans. A specificity of initial image processing for fundus reconstruction is analysed. Then, the parameterization step is performed based on the vessels segmented with the proposed algorithm. The influence of various methods on the vessel segmentation and fully automatic vessel measurement is analysed. Experiments were carried out with a set of 3D OCT scans obtained from 24 eyes (12 healthy volunteers) with the use of an Avanti RTvue OCT device. The results of automatic vessel segmentation were numerically compared with those prepared manually by the medical doctor experts.

Keywords: optical coherence tomography, image processing, mathematical morphology, vessel segmentation.

1. Introduction

The study of blood vessel distribution in the human eye retina is one of the key tests performed during comprehensive ophthalmological diagnostics. Parameterized biometric data make it easier for the ophthalmologists to analyse the lesions visible in the decomposition of fundus blood vessels [1, 2]. A quantitative analysis of vascular structure changes gives essential information about vessels' net development and any forming disorders. The important parameters used when imaging the fundus are, *e.g.*, vessel thickness, tortuosity, branching angle, and vascular density [3]. Abnormal values of these parameters signify the increased probability of various eye diseases. Also, structural retinal vascular changes may serve as indicators of the risk of cardiovascular disease [4].

A device typically used for observation and segmentation of the retina blood vessels is a so-called fundus camera, consisting of a flash lighting and a high-resolution camera. An illustrative photo obtained with this technique is shown in Fig. 1a. The resulting image has high resolution and appropriate contrast between vessels and the surrounding tissue. For this type of acquisition, there exist several techniques for segmentation of blood vessels [5], which are used for automatic (computer) or manual detection of various pathologies. An important disadvantage of fundus camera imaging is the need of applying an intense (flash) lighting when taking a picture. Therefore, for many patients such an examination causes a severe sense of discomfort.

Another technology, which can be used for the detailed analysis of the retinal vasculature, is the *optical coherence tomography* (OCT). Typically, the standard OCT devices and their software offer reconstruction of the fundus image (Fig. 1b). This is done either by using *scanning laser ophthalmoscopy* (SLO) [6] or by summation of pixel intensity values in each column of every cross-section of the 3D OCT scan (*i.e.*, in a collection of OCT B-scans, see Fig. 1c). The reason for retinal blood vessels to be visible in the OCT cross-sections is the absorption of near-infrared light by the haemoglobin molecules. This causes vessel silhouettes to appear below the position of vessels as dark shadows in the OCT B-scan images (Fig. 1c).

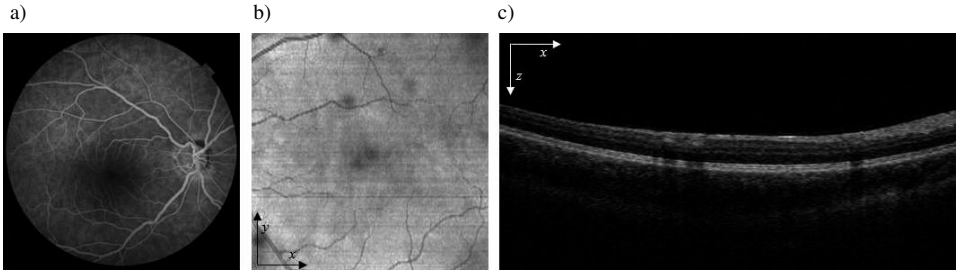

Fig. 1. Illustrative retina images: a) fundus camera image; b) fundus reconstructed from OCT; c) single OCT B-scan.

A reconstructed fundus image based on OCT has a lower contrast and signal to noise ratio in comparison with that obtained using the colour fundus photography [7]. Thus, using OCT images for vessel parameterization increases the overall process difficulty. However, an unquestionable advantage of this technology, in addition to the noninvasive examination, is the ability to precisely combine the image of the segmented vessels with the image of the retinal layers. It enables to prepare a so-called virtual fundus map for a physician planning an operation [8].

Effectiveness of segmentation of blood vessels depends of course on the image quality (the background should preferably be uniform). Moreover, the segmentation accuracy substantially depends on whether a healthy eye or an eye with anomalies (not necessarily resulting from diseases of blood vessels) is examined.

Figure 2 presents a general block diagram of both fully- [9] and semi-automatic [10] retina vessel parameterization. The main steps are vessel segmentation (performed with various algorithms) and extraction of the vessel central line. Next, for each point belonging to the central line,

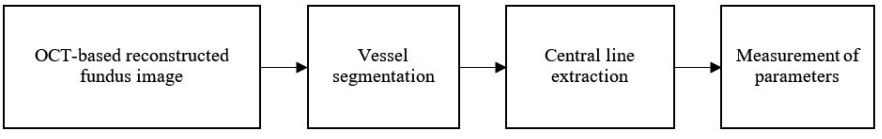

Fig. 2. A general block diagram of the retina vessel parameterization algorithms.

Metrol. Meas. Syst., Vol. 26 (2019), No. 3, pp. 449–461
DOI: 10.24425/mms.2019.129581

selected vessel parameters are measured. This applies to such characteristics as width, tortuosity, or branching angle of the vessels. The calculated values are subjected to clinical evaluation. Finally, the obtained parameter values can be used for the diagnostic evaluation.

Figure 3 illustrates an example of measuring diameter and branching angle of vessels with the use of the reconstructed fundus image. These parameters reflect the existing cardiovascular risk in the body, including angioedema, elevated blood pressure, overweight, and diabetes, and can be used in predicting, for example, stroke or cardiac diseases. Examples of anomalies in the retinal vascular net include more tortuous vessels, lower values of vascular angles, thinner arteries, and larger vein diameters [11].

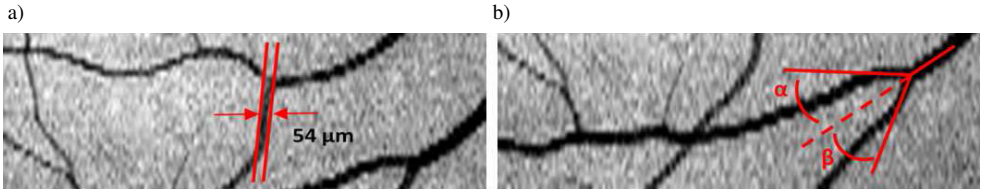

Fig. 3. Example of vessel parameters measured on the basis of reconstructed fundus image: a) width; b) division angle.

2. Segmentation of retinal vessels using OCT data

The basic step leading to the analysis of the vessels' net structure is a proper extraction of vessels from the fundus image. There are various segmentation methods dedicated to the colour fundus images. They take advantage of typical characteristics of the colour fundus images, such as high resolution and high contrast of the vessels in relation to the surrounding tissue (especially in the green monochromatic image). Further contrast enhancement can be achieved with the modification of histogram during the pre-processing stage. Repeated execution of morphological operations and image transformations gives the final extracted vessels' net [12]. A comprehensive review of both supervised and unsupervised approaches can be found in [5].

On the other hand, the OCT-reconstructed fundus image has a much lower resolution (primarily in the non-fast scanning direction), as well as a lower contrast. Such image characteristics make direct implementation of the well-established vessel segmentation methods unsuccessful. Therefore, basing on several solutions [13, 14], we propose modified procedures for vessel segmentation from the OCT-reconstructed fundus images.

In this paper, we propose three competitive approaches described in Subsection 2.3 for automatic parameterization of retina vessels segmented using OCT data. They are based on combinations of morphologic and filtering operations, namely: *Blur, Minimum, LOG* (BML, Subsection 2.3.1), *Blur, Difference, Dilation* (BDD, Subsection 2.3.2), and *Bottom Hat* (BH, Subsection 2.3.3). We present results of the tests and additionally examine the influence of a selected vessel segmentation approach on the accuracy of measured parameters.

2.1. Pre-processing

To obtain an OCT-reconstructed fundus image, the following pre-processing steps have to be performed:

– volumetric OCT noise reduction with adaptive *block matching and 4D filtering* (BM4D) [15]. This algorithm incorporates Wiener filtering of a 3D dataset, thus providing a suitable

denoising effectiveness for medical images. It also ensures contrast enhancement in 3D and reduction of nonuniform tissue brightness.

– retina layer segmentation of layers containing the superficial vascular plexus: *ganglion cell layer* (GCL) [16]; as well as hyper-reflective layers comprising shadows of those vessels: *outer photoreceptor segments* (OS), and *retinal pigment epithelium* (RPE). For selected regions upper and lower borders are segmented using our modified graph theory-based approach [17].

Figure 4 shows an example of two superficial vessels marked with two red circles. These vessels are visible as bright areas in the GCL layer and dark regions underneath (the shadows of these vessels). Blue and green curves drawn in the B-scan image represent the upper and lower boundaries of the GCL and OS+RPE layers, respectively.

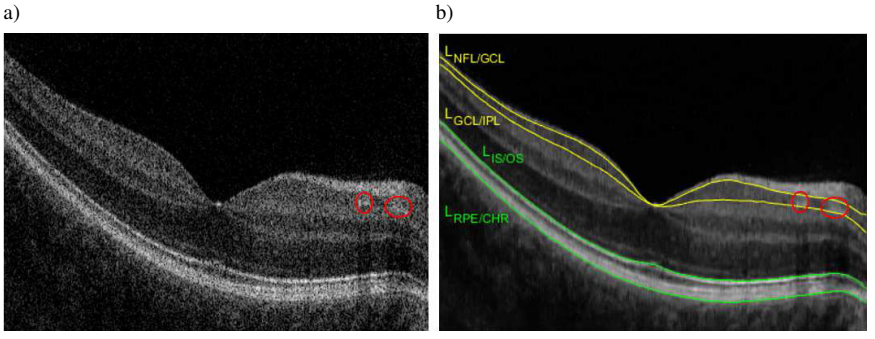

Fig. 4. Example of a) raw OCT B-scan image and b) filtered B-scan image with segmented GCL and RPE layers.

2.2. Fundus image reconstruction

The literature provides several methods for fundus image reconstruction from 3D OCT data. Early techniques, based on averaging each A-scan [18], included noise present in the area outside the examined tissue. Such a fundus reconstruction has a low contrast due to incorporating pixels with a higher reflectivity of blood cells and surrounding tissue. Other methods are based on the projection of outer retinal layers [19, 20]. This ensures a better contrast between vessel shadows and hyper-reflective tissue of RPE. Also, Hu *et al.* proposed a vessel-oriented OCT-projection image creation, which incorporates computing the mean intensity values in the region of OS and RPE layers [21].

In the performed experiments we tested two following approaches of the fundus image reconstruction. For this purpose, we established a spatial coordinate system of the processed OCT volume $I(x, y, z)$, where x and y represent pixel indexes in horizontal fast and non-fast scanning directions, and z stands for a pixel index in the vertical direction, as indicated in Fig. 1:

– vessel-oriented OCT-projection image $P_1(x, y)$ (as proposed by Hu *et al.* [21]) calculated as mean of pixel intensity values in each B-scan column from the area of hyper-reflective tissues, *i.e.*, *outer photoreceptor segments* (OS) and *retinal pigment epithelium* (RPE). Equation (1) describes this operation:

$$P_1(x, y) = P_{\mathrm{OS+RPE}}(x, y) = \frac{\sum_{z=L_{\mathrm{IS/OS}}(x,y)}^{L_{\mathrm{RPE/CHR}}(x,y)} I(x, y, z)}{L_{\mathrm{RPE/CHR}}(x, y) - L_{\mathrm{IS/OS}}(x, y)}, \tag{1}$$

Metrol. Meas. Syst., Vol. 26 (2019), No. 3, pp. 449–461
DOI: 10.24425/mms.2019.129581

where $L_{IS/OS}$ denotes the border location between the inner and outer segments of photoreceptors, $L_{RPE/CHR}$ denotes the border location between the RPE and choroid layers,

– selectively reconstructed fundus image $P_2(x, y)$ calculated as a function of the projections of GCL and OS+RPE layers, as described by (2):

$$P_2(x, y) = w_1 P_{OS+RPE}(x, y) + w_2 P_{GCL}(x, y) + \varepsilon, \tag{2}$$

where parameters w_1 and w_2 are used to weight the influence of vessels and their shadows, parameter $\varepsilon \in \langle 0,\ 1\rangle$ is used for enhancing intensity values of the projection, and the GCL projection is calculated as follows:

$$P_{GCL}(x, y) = \frac{\sum_{z=L_{GCL/IPL}(x,y)}^{L_{NFL/GCL}(x,y)} I(x, y, z)}{L_{NFL/GCL}(x, y) - L_{GCLIPL}(x, y)}. \tag{3}$$

Figure 5 shows an example of normalized P_{GCL} and P_{OS+RPE} projection images as well as P_2 projection image with enhanced contrast of small vessels. These images were obtained from 3D OCT data. It can be seen that the tissue reflectance in the GCL layer enables to emphasize vessels that exist in the superficial vascular complex and are too small to leave a significant shadow trace.

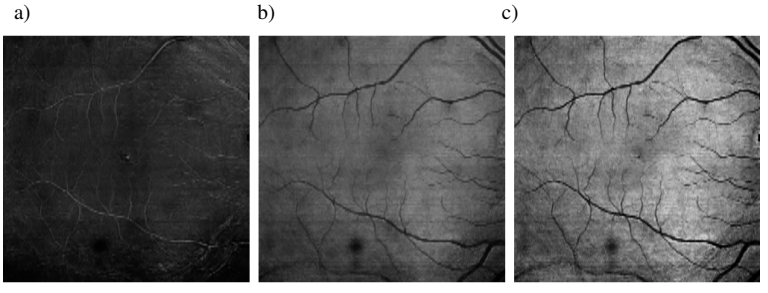

Fig. 5. Projections of layers and fundus reconstruction images using various retina regions: a) GCL layer projection; b) OS+RPE layer projection; c) P_2 fundus reconstruction from GCL and OS+RPE layers.

Available resolution of the above fundus image projections depends on the abilities and protocol of the volumetric OCT acquisition. A typical reconstructed fundus image achievable with a fixed scanning time of OCT registration results in uneven resolutions for the fast and non-fast scanning directions. For example, a 385×141 pixel resolution image represents a 7×7 mm retina area obtained using the Avanti RTvue device by Optovue Inc. USA [22]. Thus, to obtain the resulting vessel image evenly corresponding to its real geometric structure, a properly reconstructed fundus image must be resized (Fig. 5). For this purpose, we used the bicubic interpolation.

2.3. Morphologic and filtering operations for reconstruction of blood vessel structure

Vessel segmentation from OCT data needs to overcome some severe problems. Among them are low reconstructed fundus image resolution, uneven reflectivity of thick vessels in relation to thin vessels, and acquisition problems such as involuntary eye movements. Methods that can be considered to be good solutions of these problems are based on morphological operations.

Their advantage is low complexity and good efficiency [13]. We have selected three combinations of them, described below, which were then compared experimentally. The process of image segmentation with the proposed algorithms is illustrated in Fig. 6.

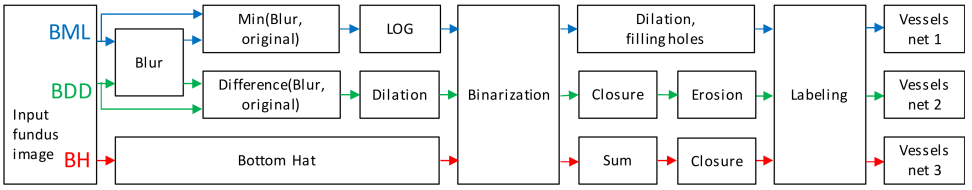

Fig. 6. A block diagram of proposed segmentation algorithms: BML, BDD, and BH.

2.3.1. BML (Blur, Minimum, LOG) combination

The first proposed method is based on three following operations: 1) blurring the input fundus image using Gauss function (Fig. 7a); 2) calculating the minimum value between the blurred and original images (Fig. 7b); 3) detection of vessel borders with an LOG (*Laplacian of Gaussian*) filter (Fig. 7c). The obtained image is then subjected to: 4) binarization with a threshold t_1 (Fig. 7d); 5) dilation and filling of holes; 6) labelling and removal of labels with the number of pixels equal to a threshold t_2 (Fig. 7e). The result is named Vessel net 1.

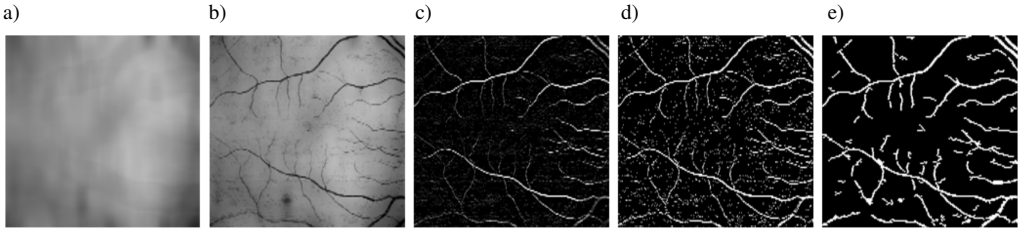

Fig. 7. BML combination: a) blur; b) minimum operation; c) LOG filtering; d) binarization; e) labelling.

2.3.2. BDD (Blur, Difference, Dilation) combination

In this method, the first step is also blurring the input image with a Gauss function (Fig. 8a). Next, we subtract the original image from its blurred version (as illustrated in Fig. 8b) to later dilate it with a linear structural element at 4 angles (0, 45, 90, 135 degrees). The maximal value of each pixel in these 4 images is chosen (Fig. 8c), and the resulting image is binarized with

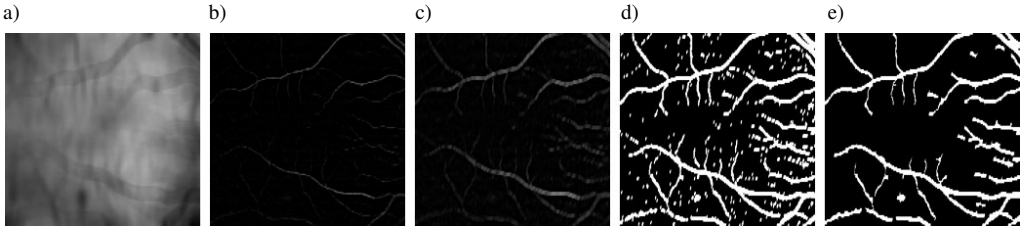

Fig. 8. BDD combination: a) blur; b) subtraction; c) dilation; d) binarization; e) labelling.

Metrol. Meas. Syst., Vol. 26 (2019), No. 3, pp. 449–461
DOI: 10.24425/mms.2019.129581

a threshold t_1 (Fig. 8d). The final step includes morphological closing and erosion, then, similarly to the BML method, labelling and elimination of small groups of pixels (with the number of pixels lower than a threshold t_2) (Fig. 8e). The result is named Vessel net 2.

2.3.3. BH (Bottom Hat) transformation

This method is based on the Bottom Hat transformation of the input fundus image. The operation is performed in 6 directions (at angles of: 0, 30, 60, 90, 120, and 150 degrees) (Fig. 9a). Then, binarization of each image with a threshold t_1 (Fig. 9b) is followed by detection of diagonal and horizontal lines, and summation of the obtained images (Fig. 9c). Finally, closing (Fig. 9d) and labelling (Fig. 9e) operations are performed. The result is named Vessel net 3.

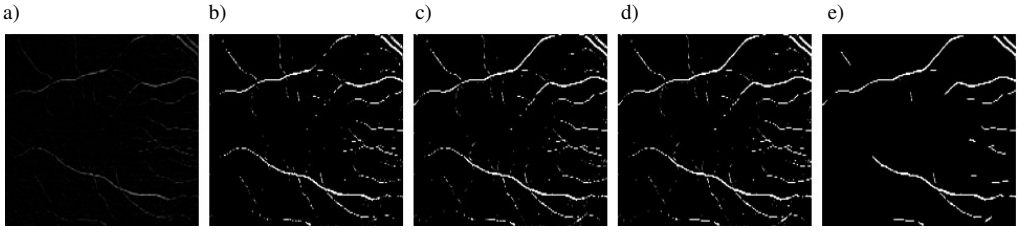

Fig. 9. BH algorithm: a) BH transformation; b) binarization; c) summation; d) closure; e) labelling.

3. Parameterization of vessels

The primary procedure for the extraction of a blood vessel from a reconstructed fundus image is the determination of the vessel central line. For this purpose, we used an algorithm for slimming elongated objects, described by Lam *et al*. [23]. It is already implemented in the Matlab/Simulink environment. In the next step selected vessel parameters are measured along the detected central lines. In this paper, we present tests of calculation of two vessel net parameters, *i.e.*, the vessel diameter and the vessel branching angle. Fig. 10 illustrates our methodology for determining these parameters. The proposed approach is described in detail in the following subsections.

3.1. Measurement of vessel diameter

Semi-automatic measurements of vascular diameters with standard procedures, *i.e.*, using a fundus camera and the resulting high-resolution fundus images, are limited to the area around the optic nerve head inside a circle of the diameter equal to three times the diameter of the optic nerve disc [24]. However, the algorithms of segmentation and measurement of vessel thickness were also tested in other areas [25].

The region of the retina examined with the OCT in the presented experiments does not merely include the optic nerve head. Therefore, the whole vascular network was checked, and the overall efficiency of vessel thickness was measured. The widths of the vessels were calculated at regular intervals of 3 pixels along the central line of the vessels. First, for each of the selected pixels, the orientation of the central line was determined by using a Matlab/Simulink build-in function *regionprops*. This function enables to calculate an angle between the x-axis and the major axis of the section of the central line in a 5-by-5 pixel region of the image. Next, using the binary image of the segmented vessel net, the diameter of the vessel was measured along the line perpendicular to the central line. The range of the measured diameters varied from 1 to 7 pixels.

3.2. Measurement of branching angle

In the process of analysis of retinal blood vessel structure, the angle of vascular branching is defined as an angle between side branches calculated in the place of disintegration [26], as shown in Fig. 10. For each of the side vessels, it is also possible to determine the distribution angles between the side branches and the main branch. The sum of them is equal to the branching angle.

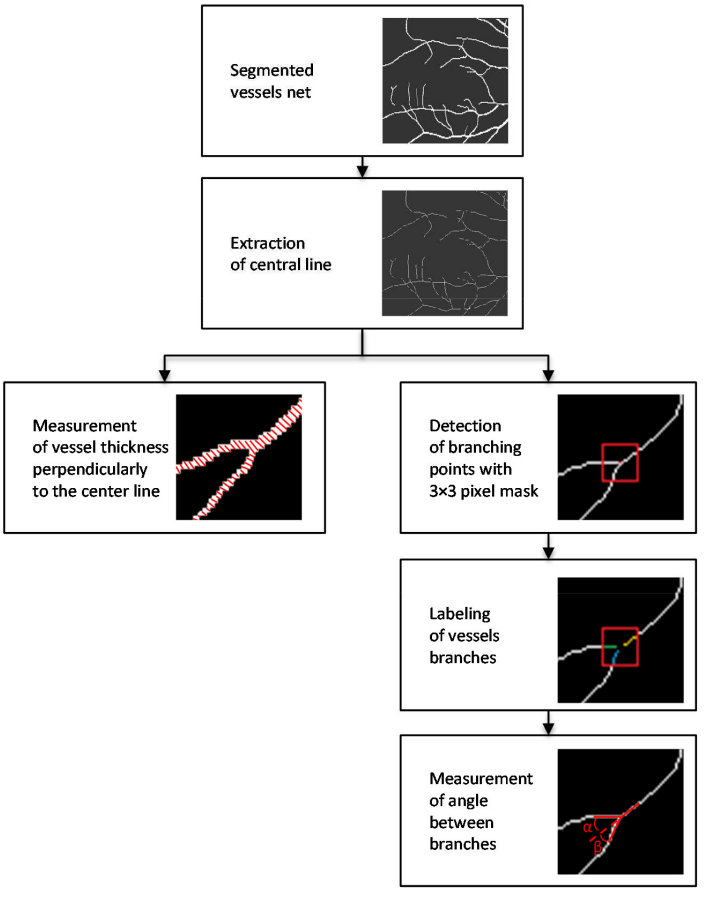

Fig. 10. Automatic parameterization of vessel structure.

In the carried out experiments, a semi-automatic method was used, in which the points of vessel separation were determined manually. The vectors located along the extracted central lines (those between the distribution angles) were 10 pixel long.

4. Analysis of vessel segmentation and parameterization accuracy

4.1. Data and experimental setup

As it was mentioned, the experiments concerning analysis of the vessel segmentation accuracy were performed using fundus images reconstructed from 3D OCT data. The OCT scans were acquired from 12 healthy volunteers (24 eyes) of 27 on average. Each 3D OCT scan consisted

Metrol. Meas. Syst., Vol. 26 (2019), No. 3, pp. 449–461
DOI: 10.24425/mms.2019.129581

of 141 × 385 × 640 data points. The device used for this purpose was an Avanti RTvue OCT (manufactured by Optovue Inc., Freemont, USA) [22]. Each volumetric dataset was subjected to retina layer segmentation with our modified graph-theory based approach [17]. Retina layer segmentation, fundus image reconstruction, and subsequent vessel segmentation were performed in the Matlab/Simulink environment with the use of Image Processing Toolbox. The resulting fundus images showed maculae with a resolution of 141 × 385 pixels.

In order to evaluate the received results of the automatic and semi-automatic vessel structure analysis, the gathered images were also manually segmented by a group of experts from the Clinical Eye Unit and Pediatric Ophthalmology Service Heliodor Święcicki University Hospital, Poznań University of Medical Sciences, to obtain the reference vessel structure. The reference vessel net was next compared with the automatically segmented retina images, to calculate the error of proposed automatic segmentation algorithms.

4.2. Results of vessel segmentation

Since the proposed methods have several parameters that need to be set, and not all of them can be selected automatically, we have analysed the reconstructed fundus images by ourselves to determine the optimal parameter values presented in Table 1. The optimization criterion was the best value of F1 score that represents the optimal values of accuracy, precision, sensitivity, and specificity [27]. Thresholds for binarization were selected from the range of $\langle 0,\ 1\rangle$.

Table 1. Optimal parameters for segmentation methods.

METHOD	OPERATION	PARAMETER	VALUE
BML	Gauss blurring	mask size	21×21
		σ	24
	Log filter	mask size	5×5
		σ	0.5
	Binarization	t_1	0.28
	Labelling	t_2	12
BDD	Gauss blurring	mask size	21×21
		σ	24
	Dilation	line size	3
	Binarization	t_1	0.12
	Closing	line size	3
	Erosion	line size	3
	Labelling	t_2	20
BH	Bottom Hat	size	3
	Binarization	t_1	0.4
	Labelling diagonal	t_2	30
	Labelling horizontal	t_2	10

Table 2 presents the results of comparison of each automatic method with the manually segmented reference vessel nets. This test illustrates the results obtained using a selectively reconstructed fundus image P_2. The data indicate that the best efficiency can be obtained with the BML method and the worst with the BH method. Low accuracy of the BDD method can be

the effect of an improper vessel thickness estimation. The BH method also results in thicker and irregular vessel lines what is reflected by lower overall score values. Fig. 11 illustrates an example of the reference vessel net and the results of proposed segmentation algorithms.

Table 2. Efficiency of automated vessel segmentation methods.

METHOD	ACCURACY [%]	PRECISION [%]	SENSITIVITY [%]	SPECIFICITY [%]	F1 score
BML	97.18	83.90	79.09	98.64	0.8156
BDD	92.35	50.84	81.06	93.20	0.6249
BH	90.69	45.04	65.59	92.96	0.5341

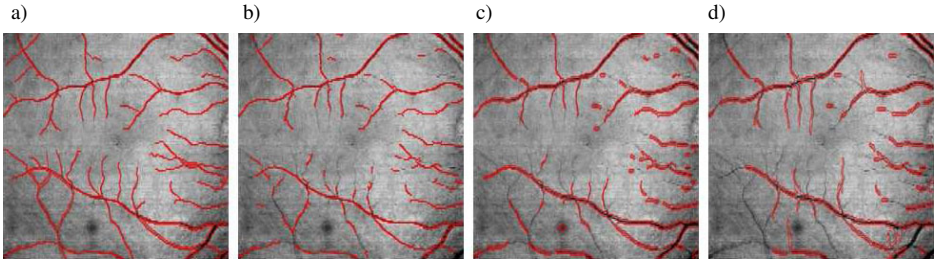

Fig. 11. Automatically segmented retina vessels overlaid in red on the fundus image for: a) reference segmentation; b) BML; c) BDD; d) BH.

Effectiveness of the methods for segmentation of blood vessels also depends on the selection of layers used for the reconstruction of the fundus image. As it is shown in Fig. 12, better results are obtained in the case of the fundus reconstructed from GCL and OS+RPE layers, but not only from the latter.

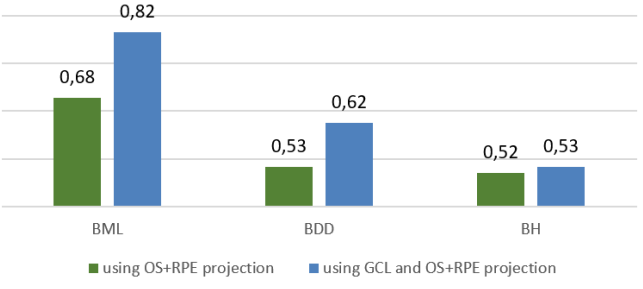

Fig. 12. Segmentation F1-score values for selected fundus reconstruction methods.

4.3. Influence of automatic vessel segmentation methods on parameterization step

The experimental studies also included analysis of the effectiveness of automatic measurements of blood vessel parameters calculated with the proposed segmentation methods. Table 3 contains the results of analysis of measurements of vascular diameter and branching angles. The measurements were performed according to the procedures described in Section 3. The analysis

Metrol. Meas. Syst., Vol. 26 (2019), No. 3, pp. 449–461
DOI: 10.24425/mms.2019.129581

was based on the comparison of parameters calculated from the automatically and manually segmented vessel structures. It illustrates the impact of the vascular network segmentation methods on the parameterization step. Table 3 shows that the best measurement efficiency was obtained for the vessel segmentation using the BML method. The BH method is the least suited for measuring the vessel parameters. The BDD method also gives worse results than the other two. As can be expected, the measurement precision is directly influenced by the resolution of the original fundus image. Thus, in a situation when an average vessel is estimated to be 3 pixels in diameter, even a 1-pixel error gives a significant difference in evaluation accuracy. It should also be noted, that even a small distortion in vessel segmentation causes a noticeable error in the branching angle measurement.

Table 3. Influence of automatic vessel segmentation method on vessel parameterization accuracy.

METHOD	WIDTH MEASUREMENT		DIVISION ANGLE MEASUREMENT	
	MSE [px]	STD. DEV. [px]	MSE [deg]	STD. DEV. [deg]
BML	3.15	1.77	12.49	21.86
BDD	17.76	3.02	17.01	21.53
BH	21.20	3.05	25.00	33.83

5. Conclusions

In this paper, we present a new approach to segmentation and parameterization of the retinal vascular net with the use of OCT examination. The proposed segmentation methods based on morphological image processing operations were selected and tested due to their marvellous effectiveness (up to 97%). Further improvement of the effectiveness is, in our opinion, still possible with the use of adaptive binarization. We plan to examine this problem in the future.

Some difficulties in the fully automatic segmentation resulted from a low contrast between the thin vessels and the surrounding tissue. Differences in segmentation regarding the vessel thickness are reflected in the obtained numerical results.

In the case of parameterization of blood vessels, it can be observed that the choice of a segmentation method is important because it directly influences the parameters of the vascular net structure description, such as the vessel diameter or angles of vascular distribution.

Currently, there is no normative database for this type of automatic measurements, and they are not performed in commercial diagnostic systems. The proposed methods as an advanced diagnostic tool can support ophthalmology specialists. In addition, the authors are currently working on a proposal to extend the existing methods with 3D OCT data analysis. This will enable to fully use the available data on the three-dimensional architecture of a vascular net.

Acknowledgments

This work was supported by the Faculty of Computing, Poznan University of Technology within the Project MODRE Number 09/93/DSMK/1901.

References

[1] Gardner, G.G., Keating, D., Williamson, T.H., Elliott, T.H. (1996). Automatic detection of diabetic retinopathy using an artificial neural network: a screening tool. *British Journal Ophthalmology*, 80(11), 940–944.

[2] Hart, W.E., Goldbaum, M., Cote, B., Kube, P., Nelson, M.R. (1997). Automated measurement of retinal vascular tortuosity. *Proc. AMIA Fall Conference*, 459–463.

[3] Cheung, C.Y., Ikram, M.K., Sabanayagam, C., Wong, T.Y. (2012). Retinal microvasculature as a model to study the manifastations of hypertansion. *Hypertension*, 60, 1094–1103.

[4] Li, L.J., Ikram, M.K., Wong, M.K. (2015). Retinal vascular imaging in early life: insights into processes and risk of cardiovascular disease. *The Journal Physiology*, 594(8), 2175–2203.

[5] Honale, S.S., Kapse, S.S. (2012). A Review of Methods for Blood Vessels Segmentation in Retinal Images. *International Journal Engineering Research & Technology (IJERT)*, 1(10), 1–6.

[6] Webb, R.H., Hughes, G.W. (1981). Scanning Laser Ophthalmoscope. *IEEE Transactions Biomedical Engineering*, BME-28(7), 488–492.

[7] Xu, J., Ishikawa, H., Wollstein, G., Schuman, J.S. (2008). Retinal vessel segmentation on SLO image. *Proc. 30th Annu Int Conf IEEE Eng Med Biol Soc*, 2258–2261.

[8] Stankiewicz, A., Marciniak, T., Dabrowski, A., Stopa, M., Marciniak, E. (2014). A new OCT-based method to generate virtual maps of vitreomacular interface pathologies. *Proc. 18th IEEE International Conference Signal Processing Algorithms, Architectures, Arrangements, Applications (SPA 2014)*, 83–88.

[9] Heneghan, C., Flynn, J., O'Keefe, M., Cahill, M. (2002). Characterization of changes in blood vessel width and tortuosity in retinopathy of prematurity using image analysis. *Medical Image Analysis*, 6(4), 407–429.

[10] Wong, T.Y., Knudtson, M.D., Klein, R., Klein, B.E.K., Meuer, S.M., Hubbard, L.D. (2004). Computer-assisted measurement of reitnal vessel diameters in the Beaver Dam Eye Study: methodology, correlation between eyes, and effect of refractive errors. *Ophthalmology*, 111(6), 1183–1190.

[11] Kandasamy, Y., Smith, R., Wright, I.M., Hartley, L. (2012). Relationship between birth weight and retinal microvasculature in newborn infants. *Journal Perinatology*, 32, 443–447.

[12] Fraz, M.M., Basit, A., Barman, S.A. (2013). Application of Morphological Bit Planes in Retinal Blood Vessel Extraction. *Journal Digital Imaging*, 26, 274–286.

[13] El Abbadi, N.K., Al Saadi, E.H. (2013). Blood Vessels Extraction Using Mathematical Morphology. *Journal Computer Science*, 9(10), 1389–1395.

[14] Mudassar, A.A., Butt, S. (2013). Extraction of Blood Vessels in Retinal Images Using Four Different Techniques. *Journal Medical Engineering*, 408120.

[15] Maggioni, M., Katkovnik, V., Egiazarian, K., Foi, A. (2013). A Nonlocal Transform Domain Filter for Volumetric Data Denoising and Reconstruction. *IEEE Trans Image Process*, 22(1), 119–133.

[16] Campbell, J.P., Zhang, M., Hwang, T.S., Bailey, S.T., Wilson, D.J., *et al.* (2017). Detailed Vascular Anatomy of the Human Retina by Projection-Resolved Optical Coherence Tomography Angiography. *Scientific Reports*, 7(42201).

[17] Stankiewicz, A., Marciniak, T., Dąbrowski, A., Stopa, P., Rakowicz, M., Marciniak, E. (2015). Improving segmentation of 3D retina layers based on graph theory approach for low quality OCT images. *Metrol. Meas. Syst.*, 23(2), 269–280.

[18] Xu, J., Tolliver, D.A., Ishikawa, H., Wollstein, G., Schuman, J.S. (2009). 3D OCT retinal vessel segmentation based on boosting learning. In: Dössel O, and Schlegel WC, editors. *Proc. World Congr Medical Physics Biomedical Engineering, IFMBE*, Munich, Germany, 179–182.

Metrol. Meas. Syst., Vol. 26 (2019), No. 3, pp. 449–461
DOI: 10.24425/mms.2019.129581

[19] Niemeijer, M., Garvin, M.K., Ginneken, B. van, Sonka, M., Abramoff, M.D. (2008). Vessel segmentation in 3D spectral OCT scans of the retina. *Proc. SPIE Medical Imaging 2008 Image Processing*, 69141R1–69141R8.

[20] Niemeijer, M., Sonka, M., Garvin, M.K., Ginneken, B. van, Abramoff, M.D. (2008). Automated Segmentation of the Retinal Vasculature in 3D Optical Coherence Tomography Images. *Investigative Ophthalmology & Visual Science*, 49, 1832.

[21] Hu, Z., Niemeijer, M., Abramoff, M.D., Garvin, M.K. (2012). Multimodal Retinal Vessel Segmentation From Spectral-Domain Optical Coherence Tomography and Fundus Photography. *IEEE Transactions Medical Imaging*, 31(10), 1900–1911.

[22] Optovue, Inc. (2016). RTVue XR 100 Avanti System. User manual. Software Version 2016.0.0.

[23] Lam, L., Lee, S.W., Suen, C.Y. (1992). Thinning Methodologies-A Comprehensive Survey. *IEEE Transactions Pattern Analysis Machine Intelligence*, 14(9), 869–885.

[24] Hubbard, L.D., Brothers, R.J., King, W.N., Clegg, L.X., Klein, R., *et. al.* (1999). Methods for evaluation of retinal microvascular abnormalities associated with hypertension/sclerosis in the Atherosclerosis Risk in Communities Study. *Ophthalmology*, 106, 2269–2280.

[25] Xu, X., Ding, W., Wang, X., Cao, R., Zhang, M., *al. et.* (2016). Smartphone-Based Accurate Analysis of Retinal Vasculature towards Point-of-Care Diagnostics. *Nature, Scientific Reports*, 6(34603).

[26] Cheung, C.Y., Tay, W.T., Mitchell, P., Wang, J.J., Hsu, W., *et. al.* (2011). Quantitative and qualitative retinal microvascular characteristics and blood pressure. *Journal Hypertension*, 29, 1380–1391.

[27] Altman, D.G., Bland, J.M. (1994). Diagnostic tests. 1: Sensitivity and specificity. *BMJ British Medical Journal*, 308(6943), 1552.